Model Reduction of a Solid Oxide Fuel Cell (SOFC) for Control Purposes

Mirabi, Emad

Department of Chemical Engineering, Tarbiat Modares University, Tehran, I.R. IRAN

Pishvaie, Mahmoud Reza*⁺

Chemical and Petroleum Engineering Department, Sharif University of Technology, Tehran, I.R. IRAN

Abbasian, Mostafa

Department of Chemical Engineering, Isfahan University, Isfahan, I.R. IRAN

ABSTRACT: *Fuel cells belong to an avant-garde technology family for a wide variety of applications including micro-power, transportation power, stationary power for buildings and other distributed generation applications. The first objective of this contribution is to find a suitable reduced model of a Solid Oxide Fuel Cell (SOFC). The derived reduced model is then used to design a state estimator. In the first step, the distributed model of the SOFC that is derived using the first principle balance equations is solved by the method of lines. Since this model is too complex and sluggish for real-time applications, a representation of this model with lower number of states and good accuracy is needed. Karhunen-Loève-Galerkin (KLG) procedure is used to develop such a reduced model.*

KEY WORDS: *SOFC, Model reduction, KLG algorithm, Distributed Parameter Systems (DPS), State estimation.*

INTRODUCTION

Fuel Cells are in limelight nowadays because of their advantages over fossil fuels and traditional methods of power generation. High efficiency, environmental friendliness and portability are among those advantages [1,2]. In fuel cells like every other process, using the model for design and control leads to better efficiency and optimum use of capacities. Since fuel cell models are a mix of complicated algebraic equations and a set of PDE's and such models are too complex to be used easily, currently fuel cells operate based on empirical knowledge. And it means that

potential of fuel cells are not fully exploited. This contribution aims to remove the obstacles lie in using such model. A reduced model will be developed which needs much less calculation time and reproduces the exact model data with high reliability.

Distributed Parameter Systems (DPS) have been studied for model reduction. *Christofides et al.* studied a particular class of DPS that exhibits two time-scale behavior (fast and slow), [3]. There it was shown that the infinite order model can be reduced to a low order finite
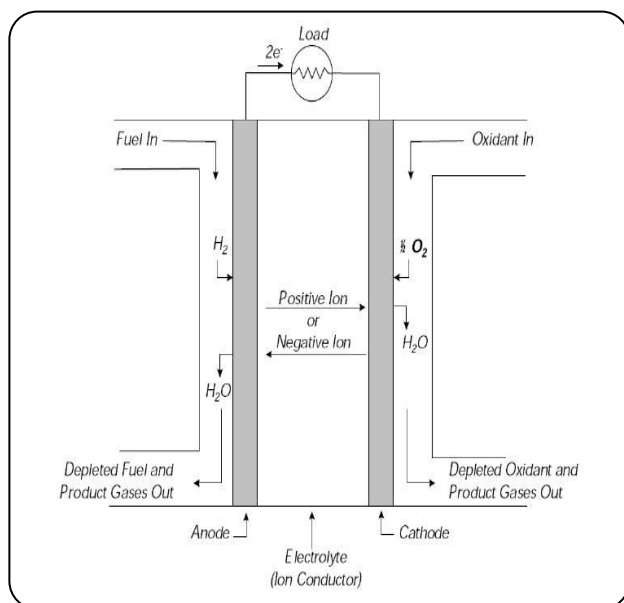
91

Fig. 1: Schematic of an individual fuel cell [11].

model that captures the dominant (slow) behavior.

Another reduction method is using the concept of Approximate Inertial Manifold (AIM) which is described in [4]. A summary of contributions of *Christofides* on nonlinear model reduction of DPS can be found in [5].

When exact description of the DPS is not available, input-output data can be used to develop a low-order model. *Gay & Ray* [6] proposed such an approach using singular function theory. The input and output data are approximated using spline functions which will be then used to find the "kernel" function that links the input to the output.

Another data-driven approach is to use Karhunen-Loève decomposition, [7]. The method was first used to reproduce stochastic field data. But it can be used to generate eigenfunctions specific to the problems. These Empirical EigenFunctions (EEF's) coupled with Galerkin method will reduce every linear and nonlinear DPS to a low order model. *Park* has used this procedure (KLG) in several distributed parameter systems with complex geometry successfully [8].

Mangold et al. have used the same procedure to develop a reduced model for a two-dimensional Molten Carbonate Fuel Cell (MCFC) system, [9]. They have also used the reduced model for parameter and state estimation of the original distributed model, [10].

This contribution aims to apply the same technique on a different type of fuel cell. The paper is organized

as follows. In next section working principle of a solid oxide fuel cell will be described briefly followed by modeling and simplifying assumptions. Other section solves the distributed model by the method of lines. Then the problem of such methods in handling the DPS and necessity of lower order models are discussed. Explanation of the KLG procedure for model reduction and its application to the distributed SOFC model are introduced in "Model Reduction" section. It is followed by testing the reliability and calculation time of the reduced model. In Designing section an observer based on the reduced model will be designed and the final section summarizes the findings.

THEORITICAL SECTION
Working principles of an SOFC

Solid Oxide Fuel Cell (SOFC) is made of two porous electrodes, an electrolyte layer between them and two gas channels outside of the electrodes. Fig. 1 shows a schematic representation of an individual fuel cell with reactant/product gases and ion flow directions. Fuel which is usually a mixture of natural gas (methane) and vapor enters the anode channel. There occur two reactions: Methane reforming and Water Gas Shift Reaction (WGSR).

Hydrogen which is produced in fuel channel uses oxygen ions and get oxidized and let out free electrons. In cathode, oxygen molecules convert to oxygen ions by consuming free electrons. The oxide ions then pass through electrolyte to reach anode. The electrochemical reaction can be briefly shown by reaction number 3 in Table 1. Free electrons transfer through a wire that connects anode to cathode and hereby electricity is produced.

One dimensional SOFC model

Distributed model of SOFC which is used in this study, with little modifications is mainly like [12].

Velocities of gases in both channels (fuel and air) are assumed to be constant. Therefore, momentum balance equations are omitted. Mass balance leads to the following partial differential equation.

$$\frac{\partial C_{ij}}{\partial t} = -\frac{\partial \left(u_j C_{ij} \right)}{\partial x} + \sum_k v_{ik} R_k \frac{1}{H_j} \qquad (1)$$

Where parameters are defined as:
C_{ij} (mol/m^3)   Concentration of component i in channel j
u_j (m/s)   Velocity of gases in channel j

92

Table 1: Chemical reactions taking place in Cell.

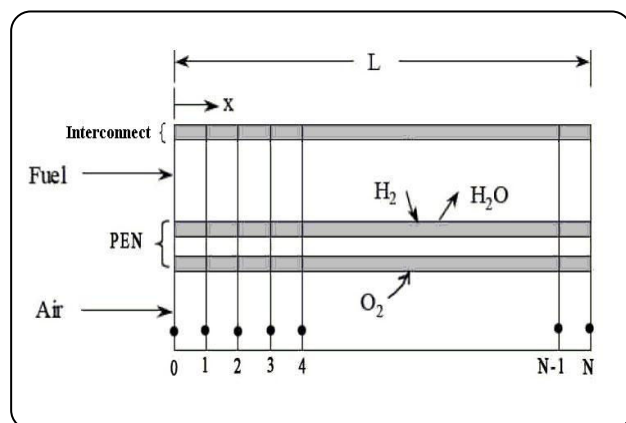| Reaction No.	Reaction Name	Chemical Equation
1	Methane Reforming	$CH_4 + H_2O \rightarrow CO + 3H_2$
2	WGSR	$CO + H_2O \leftrightarrow CO_2 + H_2$
3	H_2 Oxidation	$H_2 + (1/2)O_2 \rightarrow H_2O$

Fig. 2: Longitudinal cutting of the cell; Grid points show "Mesh-centered" approach in discretization.

R_k (mol/s.m^2)   Surface rate of reaction No. k

ν_{ik} Stoichiometric coefficient of component i
            in reaction No. k (minus for reactants)

H_j (m)   Height of channel j

Writing the above PDE for 5 components in fuel channel (CH_4, H_2O, CO, H_2 and CO_2) and 2 components in air channel (O_2 and N_2) leads to 7 PDE's. Energy balance for fuel, air, interconnect and set of electrolyte and two electrodes (which is called PEN, Positive electrode; Electrolyte; Negative electrode) gives another 4 partial differential equations. These 11 PDE's with electrochemical model (which is a set of complicated algebraic equations) constitute one dimensional model of a solid oxide fuel cell. (Complete set of model equations with parameters and operating condition can be found at the appendix)

Solving the distributed model by method of lines

In "Method Of Lines (MOL)" spatial derivatives are replaced by finite difference formulas. The accuracy of the resulting dynamic model depends on the number of grid points. "Mesh centered" approach is used in discretization, (Fig. 2). N=10, 20 and 30 were tested for the number of grid points. Solving the model in steady state and dynamic condition cleared that choosing N=10 leads to poor accuracy meanwhile N=20 and N=30 are both acceptable depending on the level of accuracy required.

In this model we have 11 PDE's and hence 11 distributed variables (7 Concentrations and 4 Temperatures). If we take N=20 (the number of grid points for each distributed variable) by method of lines, we'll have a dynamic models with 220 states. Similarly N=30 leads to a set of 330 ODEs. These models consume a lot of calculation time and are not suitable for control purposes or other real-time applications. Therefore a reduced model that accurately imitates the behavior of the system and needs less calculation time is desirable. This is one of the objectives of this paper.

Although the dynamic model which is obtained by the method of lines has too many states and is sluggish, it is very accurate and therefore it will be used as a reference to assess the accuracy of the derived reduced model. As a consequence, the expression "exact model" will be used instead of "model obtained by the method of lines" afterwards throughout this article.

Model reduction
KLG procedure

Karhunen-Loève decomposition which was first used to reproduce stochastic field data [13], here will be described briefly for reproducing data in a 2-dimensional space. It can easily be generalized for n-dimensional data. We select N arbitrary irregularly shaped numerical functions $\{\upsilon_n(x, y)\}$ which we'll call them "snapshots" afterwards.

$$\{\upsilon_n(x, y)\} \qquad n = 1, 2, ..., N \qquad (2)$$

The objective is to find the most typical or characteristic structure of these snapshots. To do this, we will start by defining C matrix.

93

$$c_{nk} = \frac{1}{N}\int_{\Omega} \upsilon_n(x,y)\upsilon_k(x,y)d\Omega \tag{3}$$

Ω is the domain where functions $\upsilon_n(x,y)$ are defined on it.

We will calculate eigenvalues and eigenvectors of the matrix C, and then we'll find eigenfunction $\varphi(x,y)$ using eigenvectors.

$$C\alpha = \lambda\alpha \tag{4}$$

$$\varphi(x,y) = \sum_k \alpha_k \upsilon_k(x,y) \tag{5}$$

Target function $\varphi(x,y)$ which will be called eigenfunctions afterwards, are assumed to be linear combinations of the snapshots.

If we sort the eigenvalues $\lambda_1 > \lambda_2 > \ldots > \lambda_N$ and the corresponding eigenfunctions $\varphi_1, \varphi_2, \ldots, \varphi_N$ in order of magnitude of the eigenvalues, then the eigenfunction φ_1 corresponding to the largest eigenvalue (λ_1) will turn out to be the most typical structure of the members of the snapshots $\{\upsilon_n\}$ and the eigenfunction φ_2 with the next largest eigenvalue (λ_2) is the next typical structure and so forth.

For different eigenvalues, it can be proven that Empirical EigenFunction (EEF's) are orthogonal.

$$\int_{\Omega} \varphi_i\varphi_j d\Omega = 0 \qquad \text{if} \qquad i \neq j \tag{6}$$

A more complete description of the method can be found in [14].

Here we use Karhunen-Loève decomposition to find basis functions in solving partial differential equations. Snapshots will be the transient response of the exact model, frozen at some specific moments and the resulting empirical eigenfunctions are taken as basis functions in Galerkin method. These problem-specific basis functions will be used in Galerkin method which is one of the methods of weighted residual to solve differential equations approximately. The combination of Galerkin method and Karhunen-Loève decomposition (KLG procedure) will reduce linear and nonlinear distributed systems to low-order lumped systems. The applicability of this procedure will not be limited by geometrical complexity of the system.

Formulation of the reduced model

Let's assume that z is a distributed variable that

satisfies the following partial differential equation.

$$\frac{\partial z}{\partial t} = b(z)\frac{\partial z}{\partial x} + c(z) \tag{7}$$

KLG procedure starts with homogenizing the boundary condition (b.c.) of z and then approximating it as a limited sum of products of eigenfunctions and amplitude temporal functions.

$$z(x,t) = U(x,t) + f(t)W(x) \tag{8}$$

U satisfies the homogeneous b.c. and W satisfies the inhomogeneous b.c.

$$U^{app} = \sum_{i=1}^{n_e} a_i(t)\varphi_i(x) \tag{9}$$

$$z^{app} = \sum a_i\varphi_i + fW \tag{10}$$

If z^{app} is substituted from Eq. (10) into Eq. (7) it doesn't exactly satisfy the PDE and a residual (Res) will remain.

$$\text{Res} \stackrel{\text{def}}{=} \frac{\partial z^{app}}{\partial t} - rhs|_{z=z^{app}} \tag{11}$$

$$\text{Res} = \sum \frac{da_i}{dt}\varphi_i + \frac{df}{dt}W - rhs\Big|_{z=z^{app}} \tag{12}$$

In Eq. (11), rhs refers to right hand side of Eq. (7).

Galerkin method of weighted residual requires that weighted integral of residual (with weighting function φ_i be zero. [15]

$$\int_0^L (\text{Res})\varphi_i dx = 0 \qquad i = 1\cdots n_e \tag{13}$$

n_e is the number of eigenfunctions that corresponds to the distributed variable "z". Later we'll discuss how n_e is determined. The integration above leads to n_e ordinary differential equations for temporal amplitude functions a_i, which will construct the reduced model.

$$\frac{da_i}{dt} = \int_0^L rhs^{app}\varphi_i dx - \frac{df}{dt}\int_0^L W\varphi_i dx \tag{14}$$

$$\frac{da}{dt} = g(a) \tag{15}$$

Hereby the partial differential Eq. 7 is replaced with n_e ordinary differential equations (Eq. 15) and this is the derived reduced model. Initial conditions are calculated as follows:

94

Table 2: Characteristics of the derived reduced model.

Var. No.	Distributed Variable	No. of eigenfunctions	No. of snapshots taken	Sum of normalized eigenvalues
1	C_{CH4}	4	68	0.999991
2	C_{H2O}	5	80	0.999999
3	C_{CO}	4	80	0.999966
4	C_{H2}	5	88	0.999998
5	C_{CO2}	4	90	0.999992
6	C_{O2}	2	35	1
7	C_{N2}	2	15	0.999999
8	T_f	5	85	0.999999
9	T_a	5	85	0.999999
10	T_{PEN}	4	90	0.999999
11	T_I	4	90	0.999999

$$a_i^0 = \frac{\int_0^L U(x,0)\varphi_i dx}{\int_0^L \varphi_i^2 dx} \tag{16}$$

If the spatial derivative in PDE (7) was of second order, it would have 2 boundary conditions and then boundary conditions could be homogenized (in the most general way) by adding a term to Eq. (8).

$$z = U + f_1 W_1 + f_2 W_2 \tag{17}$$

U again satisfies the homogeneous b.c. and W_1 and W_2 satisfy the inhomogeneous b.c.

Calculation of the empirical eigenfunctions

Since there is no systematic trend in selection of the snapshots in nonlinear systems, their selection should be done carefully. It can be proven that if snapshots are linearly dependant, C matrix will become singular. Singularity of C matrix will make the distribution of eigenvalues abnormal. This unfavorable distribution affects eigenvectors and eigenfunctions in turn. Therefore a possible criterion for selection of snapshots can be condition number. Another possible criterion that is imposed is the performance of the reduced model.

Snapshots are due to transfer the pattern to eigenfunctions. If we select more diverse snapshots, eigenfunctions recognize the structure of the distributed variable better. Table 2 shows the characteristics of the derived reduced model. Number of eigenfunctions and number of snapshots are determined for each distributed variable (7 Concentrations and 4 Temperatures).

Number of eigenfunctions is selected based on the performance of the reduced model. For variables with more complex differential equation, more eigenfunctions are needed to cover all the dynamic modes of that distributed variable.

Since i-th eigenvalue shows how i-th eigenfunction represents snapshots, sum of normalized eigenvalues gives us an index of how well snapshots are covered.

Figs. 3-13 show calculated eigenfunctions for each distributed variable. First eigenfunctions which were due to extract the most typical structure of a set of snapshots for each distributed variable have turned out to be like steady state profile of variables. Next eigenfunctions cover the dynamic modes of each variable.

Since every PDE is replaced by n_e ODE's (Eq. (15)), the order of reduced model is equal to sum of number of eigenfunctions which is 44 here.

Reliability of the reduced model

If we define an error index like this:

$$IARE_i = \int \left(\frac{\left| x_i^{exact} - x_i^{KLG} \right|}{x_i^{exact}} \right) dt \tag{18}$$

Where:

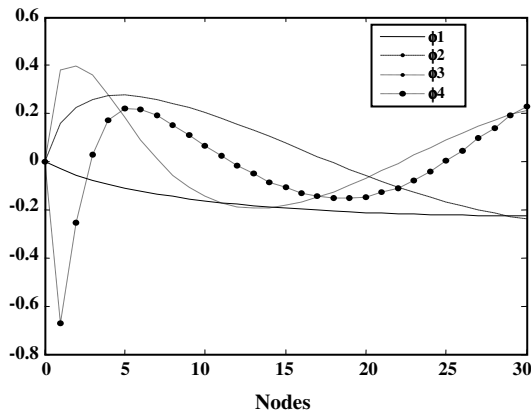|	
i	Node number
KLG	Reduced model (which is derived based on KLG algorithm)
exact	Exact model (model developed by method of lines)
x	any of the 11 distributed variables

95

Fig. 3: Empirical Eigenfunctions associated with 1ˢᵗ distributed variable (C_{CH4}) (Concentration of Methane in the fuel channel).
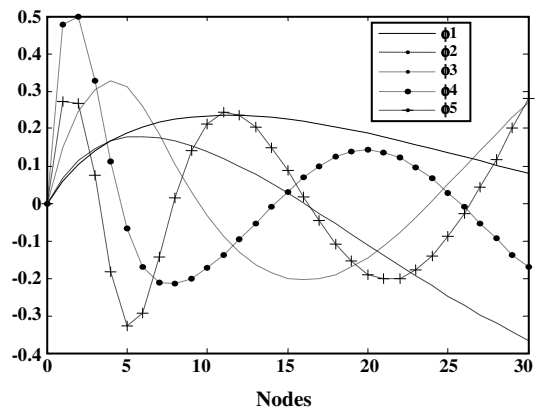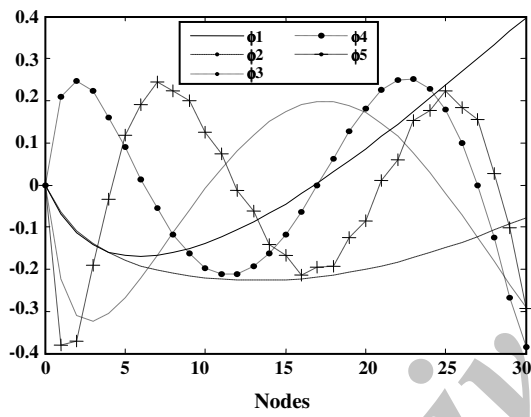

Fig. 4: Empirical Eigenfunctions associated with 2ⁿᵈ distributed variable (C_{H2O}) (Concentration of steam in the fuel channel).
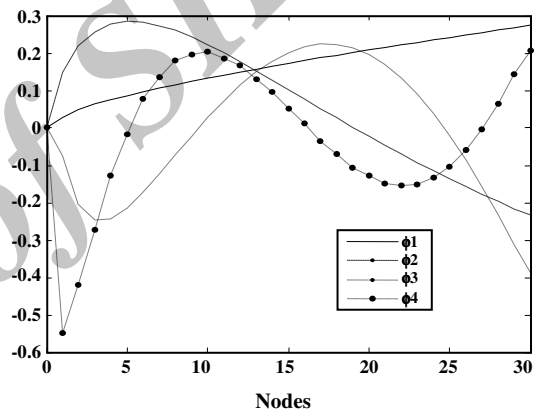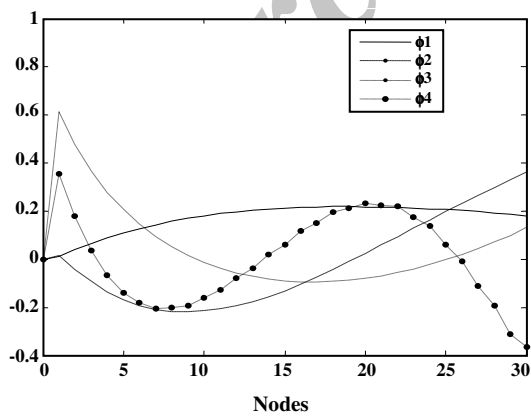

Fig. 5: Empirical Eigenfunctions associated with 3ʳᵈ distributed variable (C_{CO}) (Concentration of carbon monoxide in the fuel channel).
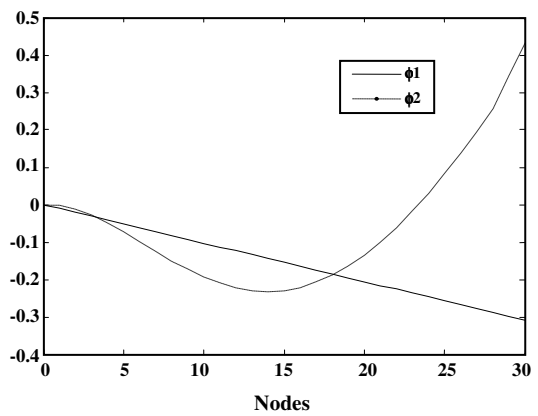

Fig. 6: Empirical Eigenfunctions associated with 4ᵗʰ distributed variable (C_{H2}) (Concentration of Hydrogen in the fuel channel).

Fig. 7: Empirical Eigenfunctions associated with 5ᵗʰ distributed variable (C_{CO2}) (Concentration of Carbon dioxide in the fuel channel).

Fig. 8: Empirical Eigenfunctions associated with 6ᵗʰ distributed variable (C_{O2}) (Concentration of Oxygen in the Air channel).
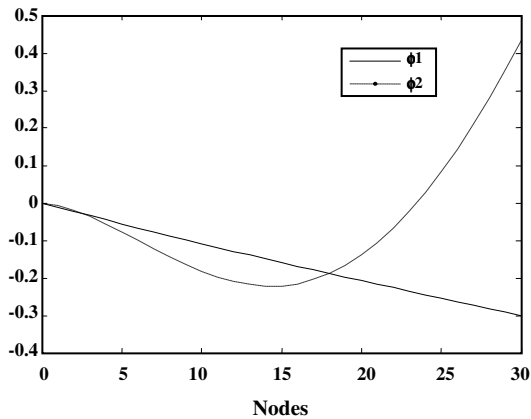
96

Fig. 9: Empirical Eigenfunctions associated with 7th distributed variable (C_{N2}) (Concentration of Nitrogen in the Air channel).
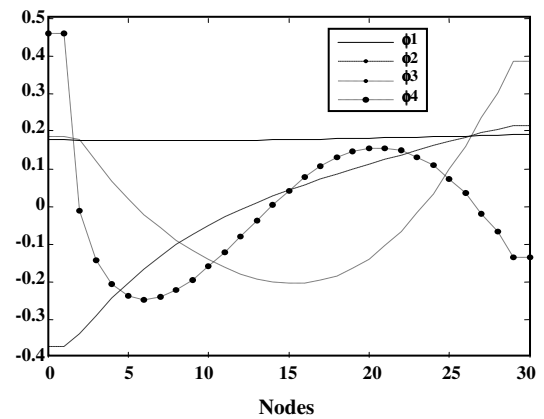

Fig. 12: Empirical Eigenfunctions associated with 10th distributed variable (T_{PEN}) (PEN temperature).
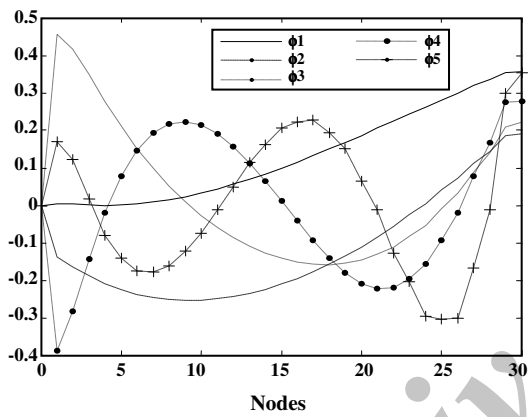

Fig. 10: Empirical Eigenfunctions associated with 8th distributed variable (T_f) (Temperature of gases in the fuel channel).
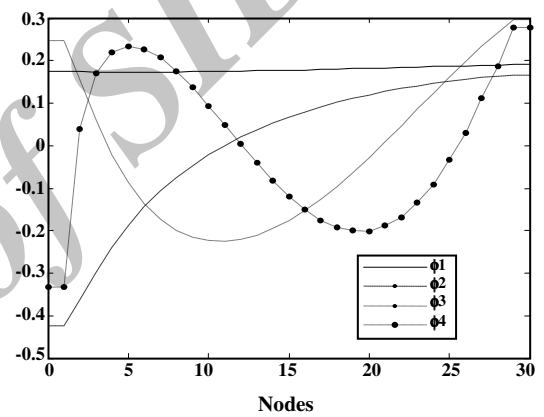

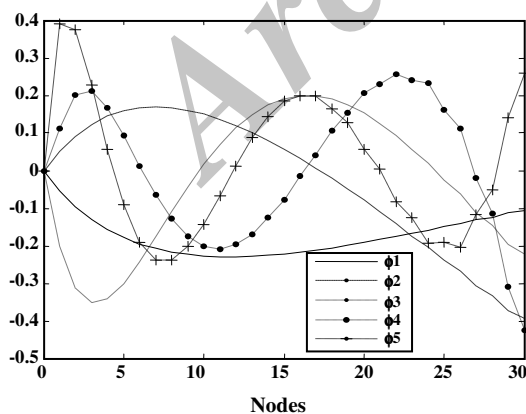**Fig. 13: Empirical Eigenfunctions associated with 11th distributed variable (T_I) (Interconnect temperature).**

Then for every distributed variable we can find 2 nodes that have best and worst performance based on the index (18). Figs. 14-24 compare reduced model and exact model for these nodes when system is excited with changes in current density.

Figures say that reduced model is of good accuracy. Moreover accurate-enough results of the reduced model ceased the process of improving it. If more accuracy is needed for one variable or for the whole model, it can be achieved by modifying eigenfunctions or the number of eigenfunctions.

Comparing the calculation time

To find out how much the reduced model is faster than the exact model, they are excited by different inputs and their simulation times are compared.

Fig. 11: Empirical Eigenfunctions associated with 9th distributed variable (T_a) (Temperature of gases in the air channel).
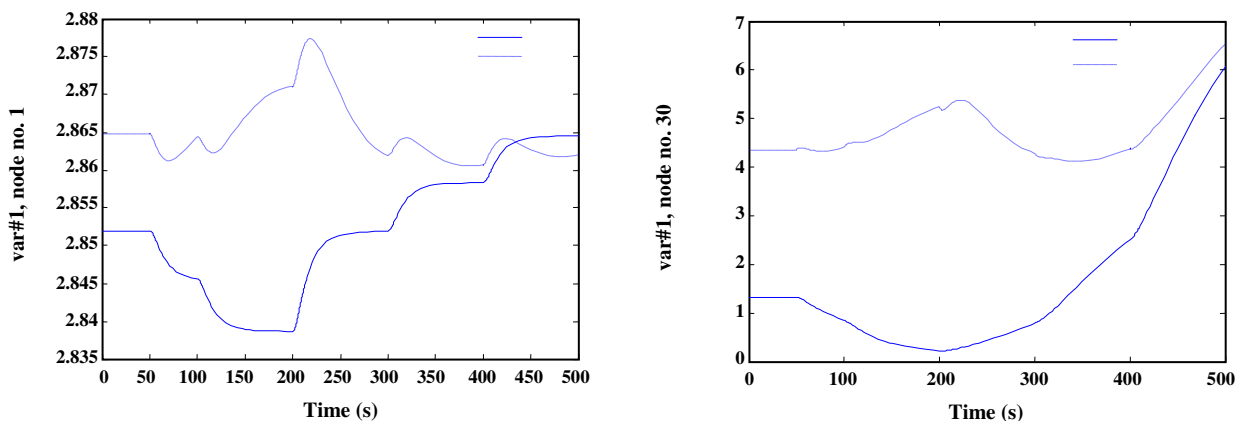
97

Fig. 14: System is excited with changes in current density and accuracy of reduced model is being assessed. Left figure shows the best and the right one shows worst performance of the 1st distributed variable based on index (18).
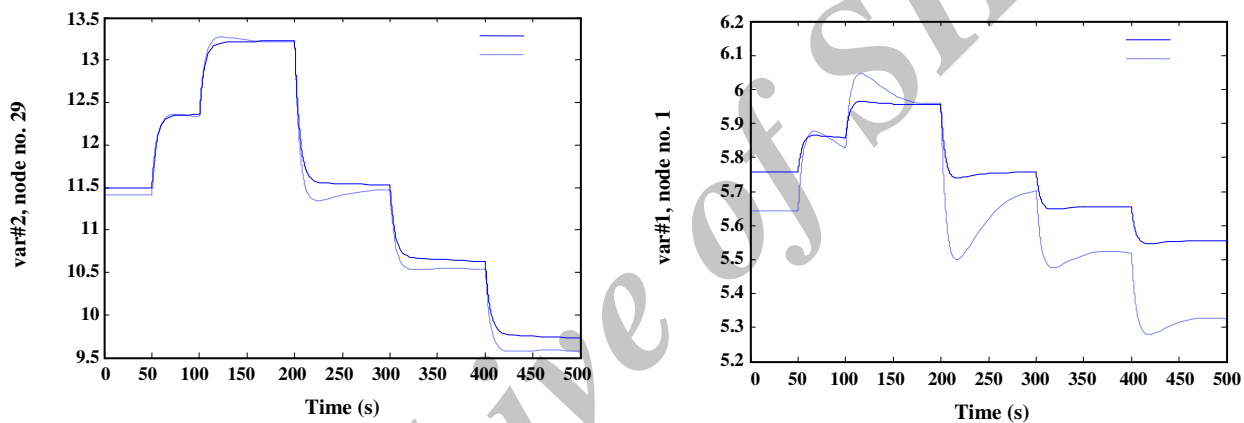

Fig. 15: System is excited with changes in current density and accuracy of reduced model is being assessed. Left figure shows the best and the right one shows worst performance of the 2nd distributed variable based on index (18)

Fig. 16: System is excited with changes in current density and accuracy of reduced model is being assessed. Left figure shows the best and the right one shows worst performance of the 3rd distributed variable based on index (18).
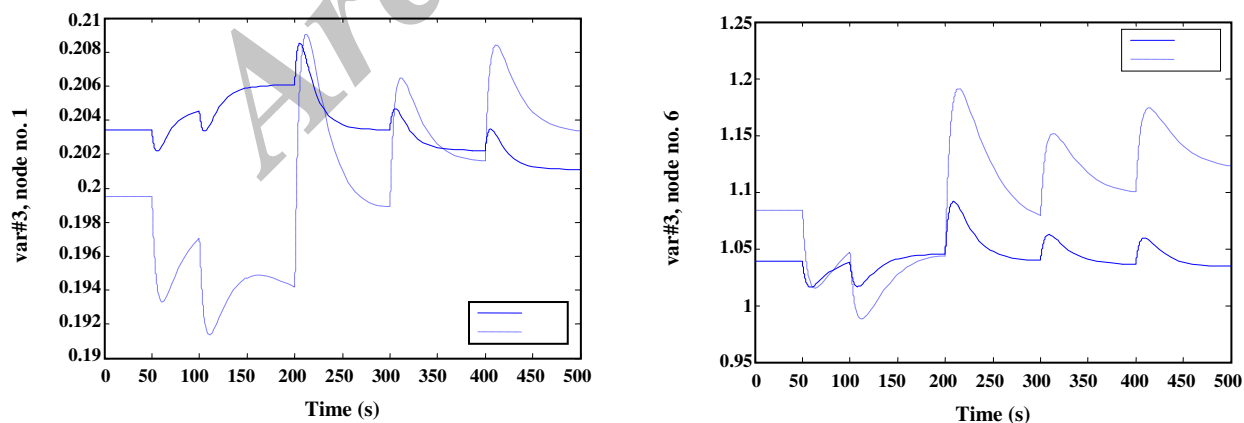
98

Fig. 17: System is excited with changes in current density and accuracy of reduced model is being assessed. Left figure shows the best and the right one shows worst performance of the 4th distributed variable based on index (18).
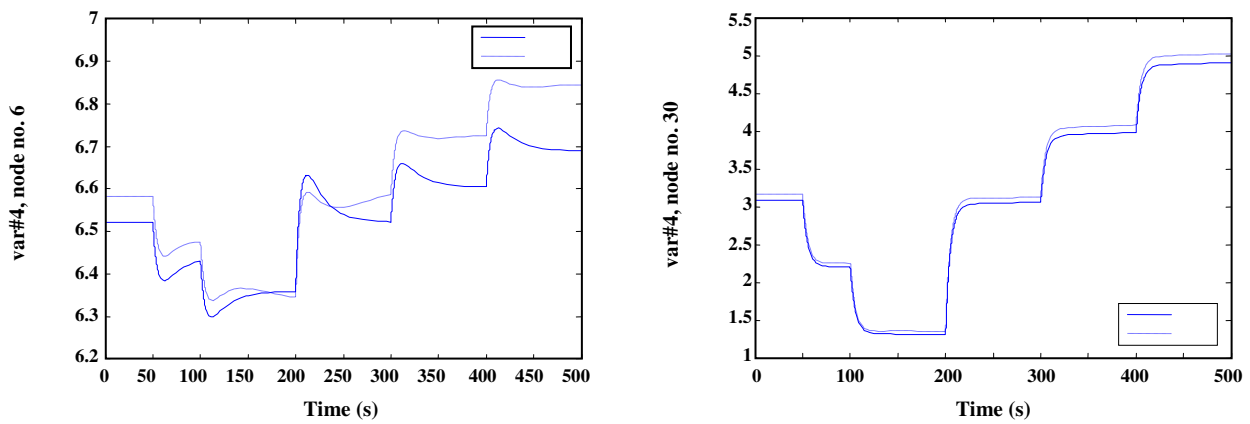

Fig. 18: System is excited with changes in current density and accuracy of reduced model is being assessed. Left figure shows the best and the right one shows worst performance of the 5th distributed variable based on index (18).

Fig. 19: System is excited with changes in current density and accuracy of reduced model is being assessed. Left figure shows the best and the right one shows worst performance of the 6th distributed variable based on index (18).
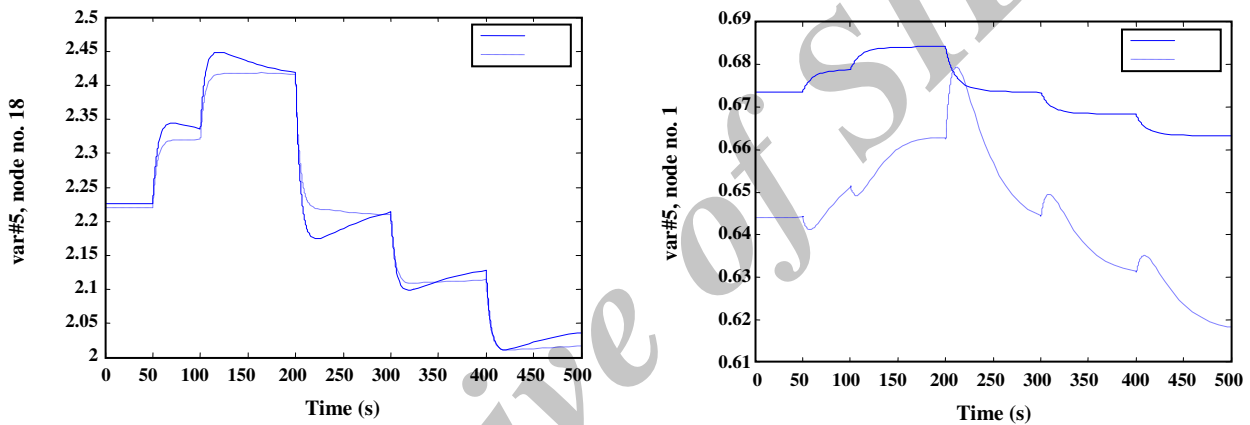
99

Fig. 20: System is excited with changes in current density and accuracy of re duced model is being assessed. Left figure shows the best and the right one shows worst performance of the 7ᵗʰ distributed variable based on index (18).
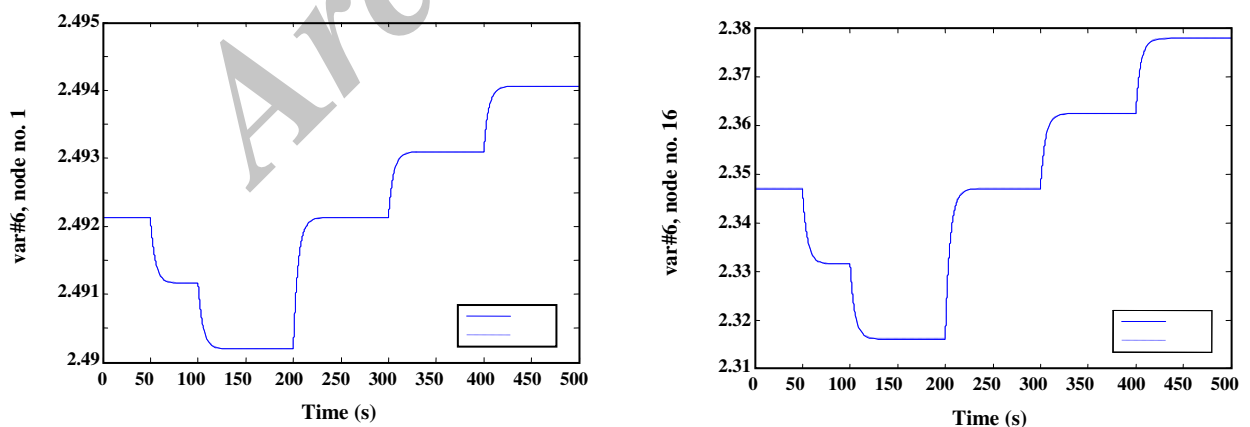

Fig. 21: System is excited with changes in current density and accuracy of reduced model is being assessed. Left figure shows the best and the right one shows worst performance of the 8ᵗʰ distributed variable based on index (18).

Fig. 22: System is excited with changes in current density and accuracy of reduced model is being assessed. Left figure shows the best and the right one shows worst performance of the 9ᵗʰ distributed variable based on index (18).
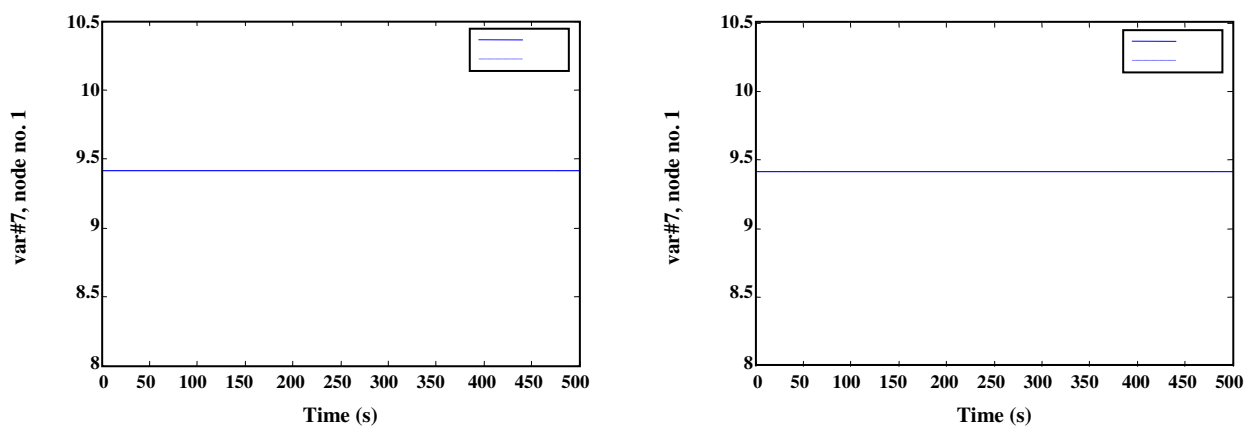
100

Fig. 23: System is excited with changes in current density and accuracy of reduced model is being assessed. Left figure shows the best and the right one shows worst performance of the 10th distributed variable based on index (18).
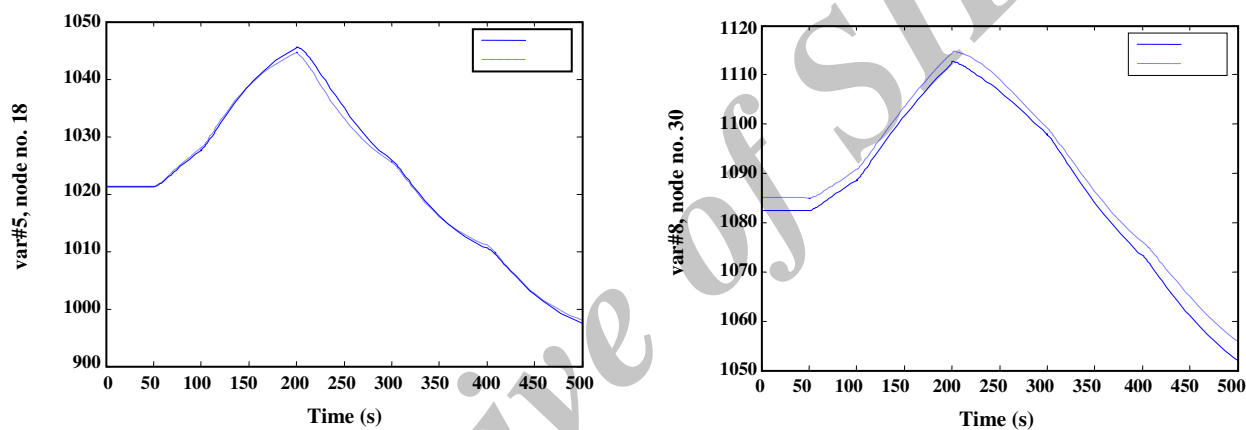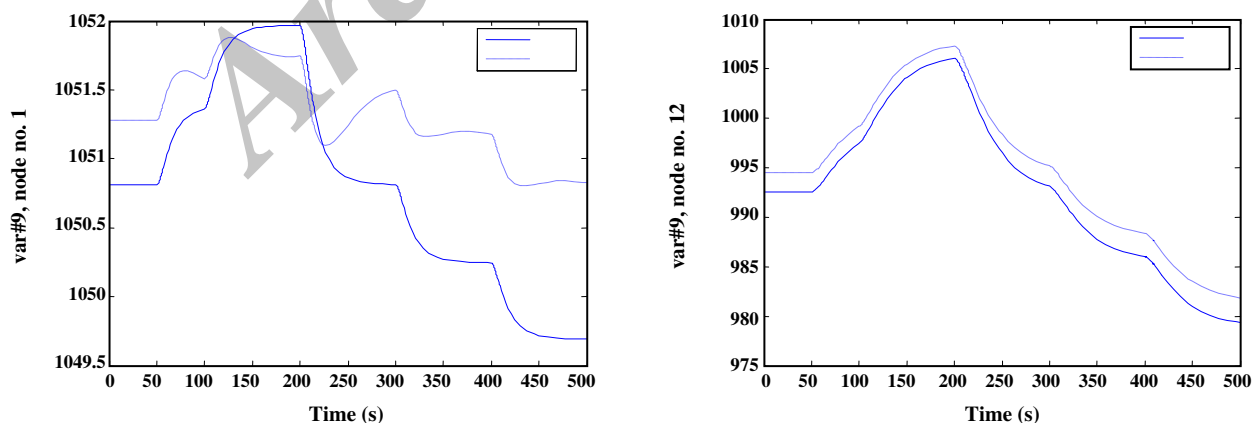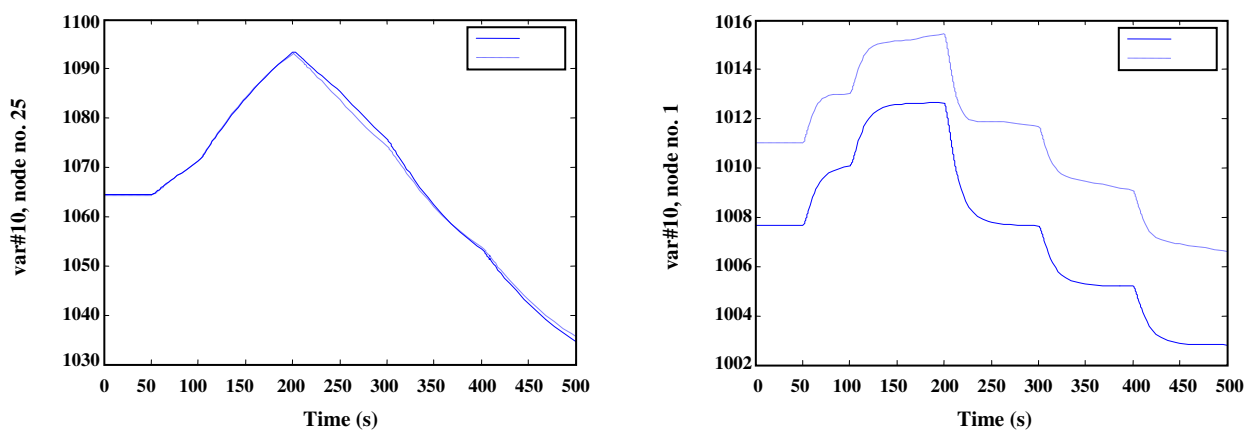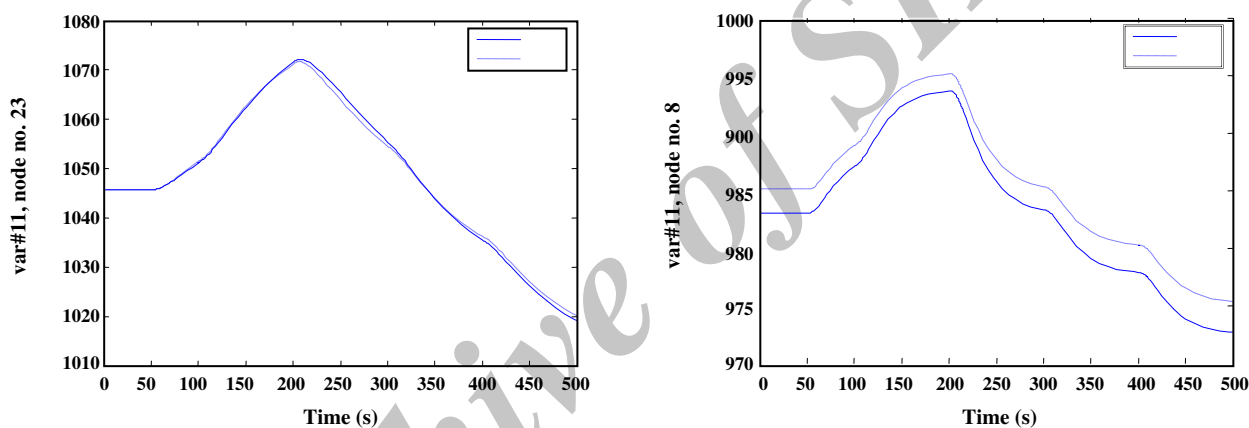

Fig. 24: System is excited with changes in current density and accuracy of reduced model is being assessed. Left figure shows the best and the right one shows worst performance of the 11th distributed variable based on index (18).
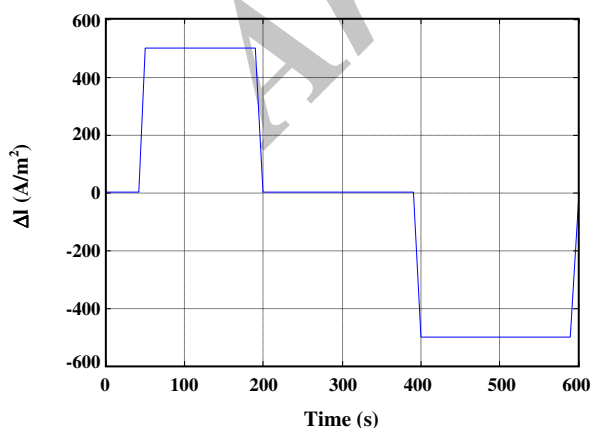
Fig. 25: Step changes in current density.

In the first case we applied changes in current density like Fig. 25. The second case is associated with 50% increase in concentration of Methane at the fuel channel input, and in the third case 100% increase in fuel velocity (Step change) is considered.

Table 3 compares the simulation time for these 3 cases. Cases 1 to 3 show 66%, 84% and 65% decrease in calculation time. The reduced model has 44 states and exact model has 330; and if we compare the calculation time by the number of states, it should have been reduced 87% but there are numerical integrations (Eq. (14)) which make the reduced model more complicated than first thought.

101

Table 3: Comparing the calculation time of reduced model and exact model for three different changes in the system.

Simulation time (sec)	KLG	MOL*
case 1	344	1014
case 2	252	1530
case 3	293	845

Fig. 26: Block diagram of observer for the SOFC.

From these 3 cases we can conclude that calculation time is reduced considerably but this reduction could be more significant if geometry of the system was more complex or the model was 2 or 3 dimensional.

Designing an observer based on the reduced model

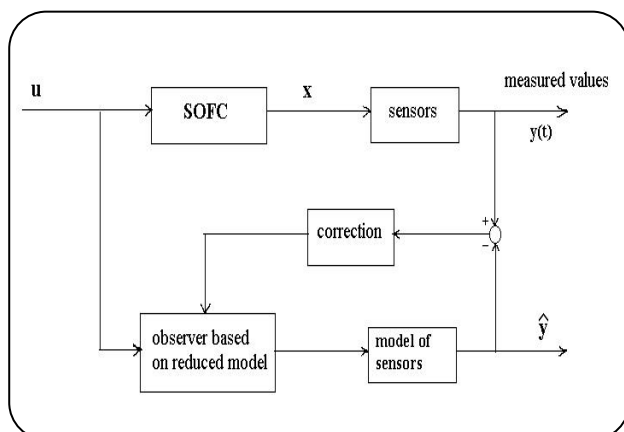To show one of the applications of the reduced model, it is used to estimate the states of the exact model. Structure of the observer is based on the reduced model and it is modified by a "correction term" like "Luenberger-like observer".

Fig.26 shows the block diagram of the observer for the SOFC system.

If reduced model is shown by

$$\dot{x} = f(x, u) \tag{19}$$

$$y = g(x, u) \tag{19}$$

Observer has the following structure.

$$\dot{\xi} = f(\xi, u) + K(y - \hat{y}) \tag{21}$$

Measured values (y in eq. 21) are provided by the exact model.

Since reduced model does not exactly reproduce exact model data, we cannot expect estimation error to converge to zero. The reduced model is a complicated nonlinear system and it is almost impossible to write it in an analytical form, therefore Lie algebra or coordinate transformation cannot be used to calculate observer gain matrix. Pole placement and Kalman filter are two linear methods which are used instead. Even if the system is not noise-corrupted we can still use Kalman filter.

To find out if the system is observable, we need to know which quantities are being measured. We take outlet temperature of fuel and air channels and average voltage as the 3 measured quantities. Linearization and calculation of A & C matrices in 2 different operating points reveals that the system is not observable. However it is detectable and therefore an observer can be designed for this system.

A linear state space equation (A & C) is detectable if there exists a matrix L so that eigenvalues of (A-LC) are negative definite [16].

Eigenvalues of matrix A (dynamic matrix of linearized system) are found to be all negative therefore even a zero gain matrix will make the linearized system detectable. Therefore nonlinear reduced model alone, without correction term (open-loop observer) will be considered as a choice.

Using Kalman filter is another way of calculating the observer gain matrix by a linear method. Matrices Q and R which are called spectral density of process and measurement noise respectively, can be used as designing parameters.

To see and compare the performance of two observers in one diagram, we'll define an error index.

$$\text{Error Index} = \left\| \overline{e} \right\|_2 \tag{22}$$

Where $\overline{e}$ is defined as follows.

e_{ki} Estimation error of distributed variable k in node i

$\overline{e}_k$ Estimation error of distributed variable k averaged along the cell

$\overline{e}$ A vector of $\overline{e}_k$ (consists of 11 elements)

Fig. 27 compares the performance of two observers in steady state condition. As expected open-loop observer is much slower than the other one.

A problem of this error index (Eq. 22) is that estimation errors of 11 distributed variables are summed
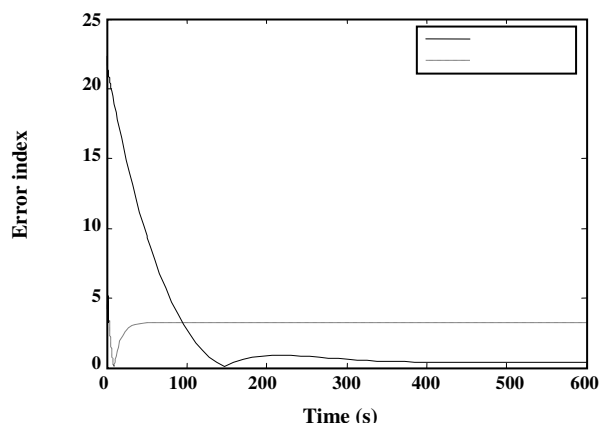
Fig. 27: Comparing performance of observers in steady state condition based on error index (22).

Fig. 28: Comparing performance of observers in steady state condition based on error index (23).

up and this way only bigger errors (which are related to temperatures) are reflected. To solve this problem, a relative error is defined.

$$\text{Relative Error Index} = \|\overline{re}\|_2 \tag{23}$$

Where $\overline{re}$ is defined as follows.

re_{ki}	Rlative estimation error of distributed variable k in node i
$\overline{re_k}$	Relative estimation error of distributed variable k averaged along the cell
re	A vector of $\overline{re_k}$ (consists of 11 elements)

Fig. 28 compares the performance of two observers based on error index (23). It is clear that Kalman filter is faster and more accurate than the open-loop observer.

To examine the performance of the observers in unsteady state condition, the system is excited with changes in current density like Fig. 25. The results are shown in Fig. 29. From Figures 27, 28 & 29 we can conclude that Kalman filter is a better choice for observation of this system.

CONCLUSIONS

In this paper, KLG algorithm for model reduction is applied on a one-dimensional SOFC model. The reduced model is then used in state estimation of the exact model. In Karhunen-Loève-Galerkin (KLG) algorithm, reduced model is developed by using the responses of the exact model. To have an exact solution, "method of lines" is applied to distributed model. Empirical eigenfunctions then calculated by having dynamic responses of the exact
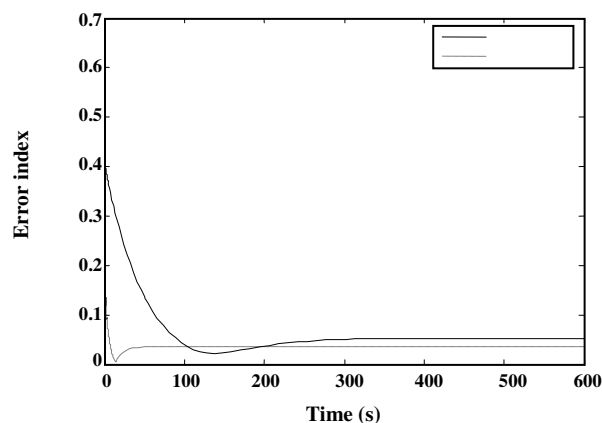
model and by applying Karhunen-Loève decomposition. These empirical eigenfunctions were used as basis functions in Galerkin method. Since it is a combination of KL decomposition and Galerkin method, the model reduction algorithm is called KLG. One of the advantages of this algorithm is that it is easily applicable on distributed systems which are defined on complex geometry.

One of the key steps in KLG algorithm is how to select snapshots. If snapshots are not rich enough, they cannot transfer dominant structures of the distributed variables to eigenfunctions and as a result the reduced model comes out inefficient and it cannot imitate the behavior of the exact model well. Although eigenfunctions and hence the reduced model are made of a limited number of transient responses of the exact model, reduced model shows acceptable behavior in different conditions and various operating points.

Comparing responses of reduced model with exact model showed good reliability and accuracy of the reduced model. Calculation time is also dropped considerably however it is predicted that if geometry of the system was more complex or the distributed model was 2 or 3 dimensional, reduction of calculation time would be more justifiable.

One of the incentives of model reduction is to use it as a representation of the original model in real-time applications such as state estimation, optimization and control. Here state estimation was practiced with the reduced model. The structure of observer is based on the reduced model and a correction term serves as a feedback
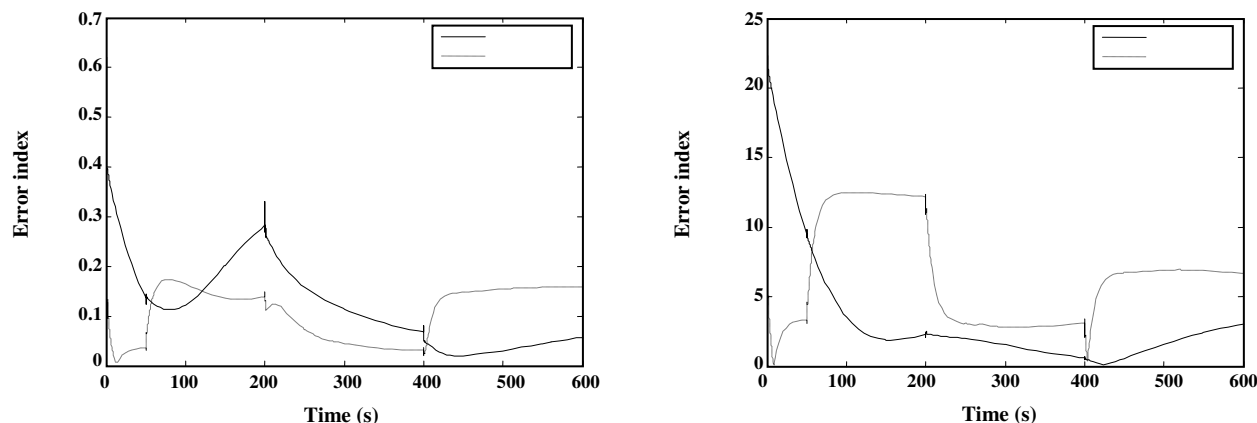
103

Fig. 29: Comparing performance of observers when system is excited based on error indices 22, 23.

signal to it. Lie derivatives and coordinate transformation couldn't be used to design an observer because the nonlinear model is not in hand in an analytical form. Instead a Luenberger-like observer was designed whose gain matrix was found by linearization and linear methods. Designed observer was examined by simulation and had acceptable performance.

Nomenclature

C_p	Specific heat capacity, kJ/kgK
C_i	Molar concentration of component i, mol/m^3
d_h	Hydraulic diameter, m
D_{eff}	Electrode effective diffusivity, m^2/s
e_a	Specific internal energy of air, J/kg
e_f	Specific internal energy of fuel, J/kg
E_a	Activation energy, J/mol
$E_{electrode}$	Activation energy of the exchange current density, J/mol
F	Faraday's constant, C/mol
F_{air}	Molar flow rate of the air stream, mol/s
F_{fuel}	Molar flow rate of the fuel stream, mol/s
h_a	Specific enthalpy of air, J/kg
h_f	Specific enthalpy of fuel, J/kg
h_i	Specific enthalpy of component I, J/kg
H_a	Air channel height, m
H_f	Fuel channel height, m
i	Current density, A/m^2
$\bar{\imath}$	Average current density, A/m^2
$i_{0,electrode}$	Exchange current density
$k_{a,I}$, $k_{a,PEN}$	Convection heat transfer coefficient of Air, J/m^{2}sK
$k_{f,I}$, $k_{f,PEN}$	Convection heat transfer coefficient of Fuel, J/m^{2}sK
k_0	Pre-exponential constant for steam reforming reaction
$k_{electrode}$	Pre-exponential factor of the exchange current density
k_{wgsr}	Arbitrary high pre-exponential factor for water gas shift reaction
K_{eq}	Equilibrium constant for water gas shift reaction
L	System length, m
n	Number of electrons participating in the electrochemical reaction
Nu	Nusselt number
P	Total pressure, Pa
p_i	Partial pressure of component i, Pa
R	Gas constant, J/molK
r_k	Rate of reaction k, mol/m^{2}s
R_{ohm}	Total cell resistance, Ω m^2
t	Time, s
T	Temperature, K
u_a	Air velocity, m/s
u_f	Fuel velocity, m/s
U_f	Fuel utilization
V	Voltage
V^{OCV}	Open circuit voltage, V
$V_{H_2}^0$	OCV for standard condition for the H$_2$ oxidation reaction, V
W	System width, m
x	Axial coordinate, m
y_i	Mole fraction of component i

Greek letters

α	Transfer coefficient
λ_{air}	Air ratio

104

λ_I	Thermal conductivity of the interconnect, J/msK
λ_{PEN}	Thermal conductivity of the PEN structure, J/msK
ε	Emissivity
$\eta_{act,electrode}$	Activation polarization in electrode, V
$\eta_{conc,electrode}$	Concentration polarization in electrode, V
η_{ohm}	Ohmic losses, V
ν	Stoichiometric coefficient
ρ	Density, kg/m^3
σ	Stefan-Boltzman constant, W/m^{2}K^4
σ_{anode}	Conductivity of anode, S/m
$\sigma_{cathode}$	Conductivity of cathode, S/m
$\sigma_{electrolyte}$	Conductivity of electrolyte, S/m
τ_{anode}	Thickness of anode, m
$\tau_{cathode}$	Thickness of cathode, m
$\tau_{electrolyte}$	Thickness of electrolyte, m
τ_I	Thickness of interconnect, m

Superscripts

0	Feed condition, standard condition
OCV	Open circuit voltage

Subscripts

a	Air
act	Activation
conc	Concentration
f	Fuel
i	Component i
I	Interconnect
k	Reaction
ohm	Ohmic
PEN	Positive electrode, Electrolyte, Negative electrode
TPB	Three phase boundary
WGSR	Water gas shift reaction

REFERENCES

[1] Seddiq M., Khaleghi H., Mirzaei M., Parametric study of operation and performance of a PEM fuel cell using numerical method. *Iran. J. Chem. Chem. Eng.*, **27**(2), (2008).

[2] Nesaraj A.S., Raj I.A., Pattabiraman R., Preparation and Characterization of Ceria-Based Elecdtrolytes for Intermediate Temperature Solid Oxide Fuel Cells (IT-SOFC). *J. Iran. Chem. Soc.*, **7**(3), p. 564 (2010).

[3] Baker J., Christofides P.D., Output Feedback Control of Parabolic PDE Systems with Nonlinear Spatial Differential Operators, *Industrial & Engineering Chemistry Research*, **38**, p. 4372 (1999).

[4] Chiu T., Christofides P.D., Nonlinear Control of Particulate Processes, *AICHE Journal*, **45**(6), p. 1279 (1999).

[5] Christofides P.D., "Nonlinear and Robust Control of PDE Systems", Boson, Birkhauser (2001).

[6] Gay D.H., Ray W.H., Identification and Control of Distributed Parameter Systems by Means of the Singular Value Decomposition, *Chemical Engineering Science*, **50**, p. 1519 (1995).

[7] Sirovich L., Turbulence and the Dynamics of Coherent Structures Parts I–III, *Quarterly of Applied Mathematics*, **45**, p. 561 (1987).

[8] Park H.M., Kim T.H., Cho D.H., Estimation of Parameters in Flow Reactors Using the Karhunen-Loeve Decomposition, *Computers and Chemical Engineering*, **23**, p. 109 (1998).

[9] Mangold M., Sheng M., Nonlinear Model Reduction of a Two Dimensional MCFC Model with Internal Reforming, *Fuel Cells*, **4**, p. 68 (2004).

[10] Mangold M. et al., Development of Physical Models for the Process Control of a Molten Carbonate Fuel Cell System, *Chemical Engineering Science*, **59**, p. 4847 (2004).

[11] Corporation, EG&G Technical Services and Science Applications International, "Fuel Cell Handbook". 6th ed., US Department of Energy, Morgantown, (2002).

[12] Aguiar P., Adjiman C.S., Brandon N.P., Anode-Supported Intermediate Temperature Direct Internal Reforming Solid Oxide Fuel Cell. I: Model-Based Steady-State Performance, *Journal of Power Sources*, **138**, p. 120 (2004).

[13] Loève M., "Probability Theory", Van Nostrand, Princeton, (1955).

[14] Park H.M., Cho D.H., The use of the Karhunen-Loève Decomposition for the Modeling of Distributed Parameter Systems, *Chemical Engineering Science*, **51**, p. 81 (1996).

[15] Finlayson B.A., "The Method of Weighted Residuals and Variational Principles", Academic Press, New York, (1972).

[16] Williams R.L., Lawrence D.A., "Linear State-Space Control Systems",John Wiley and Sons, Hoboken, (2007).

105